A numerical study on regular detonation structure and its evolution through the cell

X Y Hu [a] D L Zhang [b] B C Khoo [a] Z L Jiang [b]

[a] *Singapore-MIT Alliance, National University of Singapore, 4 Engineering Drive 3, 117576, Singapore*

[b] *Laboratory of High Temperature Gas Dynamics, Institute of Mechanics, Beijing, 100080, China*

Abstract

This paper reports results on two dimensional numerical simulation of cellular detonation wave of $H_2/O_2/Ar$ mixture with low initial pressure using detailed chemical reaction model and high order ENO scheme. A regular cellular structure develops from the one dimensional detonation wave after introduction of small random disturbances. The calculations are carried out using different grid sizes, and clear and well defined strong type structure and numerical detonation cells are obtained with high resolution calculations. Several aspects of the structure evolution through the cell are then discussed, such as shock configuration movement, pressure variation, ignition mechanisms and detonation velocity fluctuation.

Key words: Detonation, Cellular structure, Numerical simulation

1 Introduction

It is well known that gaseous detonation wave has cellular structure. Experiments show that smoked foils on channel wall can record the tracks of cellular structure, and the regions enclosed by the tracks are called detonation cells. For regular cellular structure, which are rectangular and planar modes, these can be idealized to two dimensional approximately. The structure is usually complex and involves triple shock configurations, one of which includes an incident shock wave, a Mach stem and a tvansverse wave. The structure is complicated and its details is not so easily captured or determined by experiments. Despite this, two types of structures are generally observed or indicated. In a weak type structure, the transverse wave is a non-reaction shock wave while the transverse wave of a strong structure can lead to strong ignition. Based on the evolution properties of the structure through the cell, the detonation is

classified as either ordinary or marginal. An ordinary detonation is nominally characterized by an average detonation velocity close to C-J value that is, D_{CJ}, while a marginal one attains only about $0.85D_{CJ}$. On the other hand, experimental investigations have also indicated that an ordinary detonation velocity fluctuates between $1.2 - 0.85D_{CJ}$ through the cell and a marginal detonation velocity varies from $1.4 - 0.7D_{CJ}$ (Fickett and Davis 1979).

From the late 1970's, numerical simulation has been employed to study the cellular structure (Taki et al, 1978). In the early works, simple one or two-steps chemical reaction model were used. Fine spatial resolution numerical simulation with simple reaction models have also been attempted(Quirk 1993, Gamezo et al 1999). The calculated structure showed a typical triple shock configuration, but the configuration details have not been fully resolved. Subsequently, multi-step, detailed reaction model have been used to calculate the detonation of $H_2/O_2/Ar$ mixture. With this model Lefebvre and Oran (1995) and Oran et al (1998) obtained structure of the strong type, in which strong ignition is found behind the transverse wave. For the structure evolution through the cell, Lefebvre and Oran's (1995) results indicated that between two successive triple collisions, the structure evolves form the weak type to the strong type. Furthermore, Oran et al (1998) suggested that there is energy release associated with the transverse wave only during the strong type configuration, which starts from about two-third of the way through the cell. They also calculated the instantaneous detonation velocity fluctuation through the cell, and found that the detonation velocity decay is close to that of ordinary detonation but the triple collision resemble more closely that of the marginal detonation. These two works show that the numerical detonation wave indicates the combined characteristics of ordinary and marginal detonation. However, the high resolution results obtained from simple chemical reaction model in Sharpe (2001) showed that even though the structure has a double-Mach like shock configuration, there is no strong ignition found behind the transverse wave. When the structure evolves through the cell, the distinct configuration change indicated in Lefebvre and Oran (1995) has not been found. Furthermore, Sharpe (2001) suggested that these disagreement was simply due to the previous simulation employing under-resolved meshes of the reaction zone.

In this paper, further studies on the two dimensional cellular detonation of $H_2/O_2/Ar$ mixture with detailed reaction model are to be performed. In current work, in order to ensure enough nodes to resolve the reaction zone, the cellular structure and detonation cells are calculated with much higher resolution than that of Lefebvre and Oran (1995) and Oran et al (1998). The present work is to focused on studying the cellular structure details and its evolution properties through the cell.

2 Governing equations and reaction model

The governing equations for two dimensional gaseous detonation with N species, multi-step chemical reaction model are

$$\frac{\partial \mathbf{U}}{\partial t} + \frac{\partial \mathbf{F}}{\partial x} + \frac{\partial \mathbf{G}}{\partial y} = \mathbf{S}, \tag{1}$$

This set of equations describes the conservation of density ρ, momentum $\rho\mathbf{v} \equiv (\rho u, \rho v)$, total energy density E, and density of species $\{\rho_i\}$, where $i = 1, N$. To close this set of equation, the total energy density is defined as

$$E = \rho h - p + \frac{\rho(u^2 + v^2)}{2}, \tag{2}$$

where enthalpy h and pressure p are calculated by thermochemical relation $h = h(\rho_i, T)$ (Stull, 1971), and equation of states $p = p(\rho_i, T)$ for a perfect gas, respectively.

For chemical reaction model with K elementary reactions, $k = 1, K$, the chemistry can be described by

$$\sum_{i=1}^{N} \nu_{ik}^{'} \chi_i \rightleftharpoons \sum_{i=1}^{N} \nu_{ik}^{''} \chi_i, k = 1, K, \tag{3}$$

where χ_i is the chemical symbol for species i, and $\nu_{ik}^{'}$ and $\nu_{ik}^{''}$ are molecularities of species i in kth reaction for reactants and products, respectively. The production rate of each species is given by

$$\dot{\omega}_i = W_i \sum_{k=1}^{K} (\nu_{ik}^{''} - \nu_{ik}^{'}) RP_k, \tag{4}$$

where W_i is molecular weight, and RP_k is the rate of progress variable of kth elementary reaction. In this paper, a 9 species, 19 elementary reactions model is used for hydrogen-oxygen combustion (Wilson and MacCormack, 1990). The reacting species are H_2, O_2, H, O, OH, H_2O_2, HO_2, H_2O, and 70% argon dilute is added to the gas mixture. This gas mixture is selected for numerical simulation primarily because fairly extensive studies on such mixture at low pressure showing regular detonation structure and detonation cells are produced and useful for our comparisons (Fickett and Davis, 1979).

3 Numerical Method

This set of coupled partial differential equations is solved by time-step splitting scheme which couples the Euler equations to the chemical reactions (Oran and Boris, 1987). The contribution from the fluid dynamic terms is firstly calculated to get an intermediate value $\tilde{U}$. This is followed by accounting for the source terms contribution to evaluate U in the next step. This approach allows separate solution of fluid dynamic terms and source terms with different time steps. The implication is that fluid dynamic terms can be integrated by Δt_{fluid} consistent with their CFL condition, and the source terms integrated by a stiff solver valid for chemical kinetic ODE equations by Δt_{source} with required accuracy.

In this paper, the finite difference scheme is based on 3rd order ENO-LLF scheme (Shu and Osher, 1989). For the 2nd and 3rd order terms, a modification is made by which a weighted average is used in place of the two candidate divided differences,

$$\begin{aligned} D_- &= D\left[x_{j-1/2}, ..., x_{j+l-1/2}\right] \\ D_+ &= D\left[x_{j+1/2}, ..., x_{j+l+1/2}\right], l = 2, 3 \end{aligned} \tag{5}$$

hence ensuring the smoothness of the interpolation (as opposed to the original choosing of the quantity with smaller absolute value). That is

$$D = \frac{D_+ W^+ + D_- W_-}{W_+ + W_-}, W_+ = D_-^4, W_- = D_+^4. \tag{6}$$

The above is in fact rather similar to WENO (Jiang and Shu, 1996), but in a much simpler form.

Time discretization for fluid dynamic terms is 3rd order TVD Runge-Kutta method (Shu and Osher, 1989). For chemical kinetic integrations, the set of coupled source terms is solved by Selected Asymptotic Integration Method (SAIM), which is a 2nd order accurate algorithm for solving stiff system of ODEs associated with chemical reactions (Young, 1979). Temperature is solved implicitly by iterating between equation of state and thermochemical relation after each Δt_{fluid}. However, for higher accuracy chemical kinetic integrations, temperature is also updated after each Δt_{source}. As the total energy does not change in the midst of concentration changing with chemical reaction, temperature is calculated by the same method (Fedkiw et al, 1997).

4 Computational setup and initialization

The numerical simulation models a detonation propagating through a $20mm$ height channel from left to right in a stoichiometric $H_2 - O_2$ diluted with 70% argon with initial pressure and temperature given as 6.67kPa and 298K, respectively. Firstly, one dimensional detonation is initialized by a strong shock wave, and which comes to a steady detonation velocity of about $1625m/s$ which is very close to C-J value (Gordon and McBride 1971). Then, the solution is placed on a two dimensional grid serving as the initial conditions for the two dimensional calculation.

In order to keep the detonation front within the computational domain, the grid is set to move at about detonation velocity in the positive x-direction. The right-hand boundary condition is kept in quiescent state. As discussed in Gamezo et al (1999), the left-hand boundary condition is an extrapolated outflow with a relaxation coefficient of 0.05. The boundary conditions imposed on the upper and lower boundaries are symmetry conditions, which correspond to the reflecting channel walls. The moving grid speed is set at a quantity slightly smaller than the steady detonation velocity. To keep the detonation front from crossing the boundary, the solution are transferred to a spatial location at a short distance on the left when the front is too closed to the right boundary. In this way, the numerical detonation wave is thus observed for very long physical time and ensured free from the effect of initial condition with imposed perturbations. The grid size used for calculating the formation process of regular cellular structure is $0.2mm$. The results are then projected onto smaller size grids, which are $0.1mm$, $0.05mm$ and $0.025mm$ for further calculations. The smallest grid size is about one sixth of that in Lefebvre and Oran (1995), which gives about 70 node points for the reaction zone. In all the cases, spatial steps are the same in the x and y directions.

The initial condition is perturbed by introducing random disturbances to the initial states only for the first time-step of chemical kinetic integrations via

$$e^* = e + \alpha e f. \tag{7}$$

Here e^* is the perturbed total specific energy which encompasses the small fluctuations to the direction of elementary reactions, f is a random value uniformly distributed in $[-1.0, 1.0]$ and α is a fluctuation coefficient of $0 < \alpha < 1.0$, controlling the fluctuation amplitude.

5 Results and discussion

5.1 Regular cellular structure

The numerical results show that the initial disturbances are indeed very small. In Fig. 1a, one can hardly distinguish the difference from the perturbed pressure contours. However, as the detonation propagates, the disturbances are magnified, and it is observed the existence of transverse waves, Mach stems and incident waves which give rise to the triple wave configurations at about $15\mu s$ (see Fig. 1b). Eventually, after a time of about $1ms$, the structure becomes very regular with equilibrium but less transverse wave number than the earlier time. Figure 1c shows the pressure contours of the regular cellular structure at $2.072ms$. One can find that, in the current work, the transverse wave number formed is 5. It is noted that the detonation runs at a average detonation velocity of 1625m/s, the same as that of one dimensional detonation.

The grid resolution study next shows that the global features, such as the average detonation velocity and the transverse wave number, are the same for all the different cases. However, the flow field is characterized by increasing levels of detailed feature revealed when the smaller grid sizes are used. Figures 2 and 3 show the pressure, density, temperature and H_2O concentration with grid size $0.2mm$ and $0.025mm$, respectively. In both figures, the transverse wave is at about the half-way mark of two successive triple collisions. From the results with $0.2mm$ grid size, one can perceive the presence of the triple wave configuration, but the configuration details is unclear. There seems to be a slip line dividing the region behind the Mach stem and the transverse wave, but is not well defined (see Fig. 2b, 2c). As shown in Fig 3, the previous unclear configuration has seen vast improvement much in results with $0.025mm$ grid size. One can find that the triple wave configuration is very clear and showing a complex shock configuration, in which the transverse wave can be divided further into three parts: the weak transverse wave, the strong transverse wave and the extending transverse wave. The former two parts have straight shock fronts while the latter is an expanding shock which connects the strong transverse wave by a kink and decays along the extending direction (see Fig. 3a). Very strong ignition (shown as sharp discontinues of H_2O concentration in Fig. 3d) are found behind the Mach stem and the strong transverse wave while less strong ignition is also found behind the incidental wave and the weak transverse wave. It is observed that the ignition is completed within the region close to the leading front. For the extending transverse wave, no ignition occurs as its front is lagged at a distance behind the ignition front of the incident wave. Other details only resolved by the high resolution results are the regions of instabilities. One can find that the slip line is unstable and produces a strong

vortex. Another instability occurs in the reaction zone after the incident wave. It is noted that these instabilities do not effects the cellular structure evolution and the other global features.

The calculated shock configuration is consistent with previous experimental observation on spin and planar marginal detonations in which the transverse waves have different parts (Schott 1965, Voitsekhovskii, Mitrofanov and Topchian 1966). The H_2O concentration in Fig. 3d is also consistent with the recent experimental observation (Shepherd et al 2003) on the reaction zones of ordinary detonations in the same gas mixture. In Lefebvre and Oran (1995) and Oran et al (1998), similar transverse wave properties were suggested but not so well defined probably due to their much lower resolution calculations. It can be found that the present shock configuration is stronger than the double-Mach like configuration obtained with simple chemical reaction model in Sharpe (2001). The main difference is that, in the present configuration, the transverse wave is stronger and there is a kink between the strong transverse wave and the extending transverse wave. In addition, strong ignition is found behind the present strong transverse wave while there is an absence of strong ignition behind the transverse wave in Sharpe (2001). As complex shock configuration has been found in current structure, according to the structure type definition in Fickett and Davis (1979), such said structure is considered to be of the strong type. However, this strong type structure seems weaker than that of a typical marginal detonation wave which has stronger and longer strong transverse wave front, and even consists one or more transverse wave parts with straight front at the location of the extending transverse wave (Voitsekhovskii, Mitrofanov and Topchian 1966).

5.2 Detonation cells

To obtain detonation cells, we use flow speed $|\mathbf{v}|$ of the numerical results to simulate the smoke foil experiment. Hence, the maximums of $|\mathbf{v}|$ on all grid nodes in the time history

$$|\mathbf{v}|_{max,i,j} = \left[\left(\sqrt{u^2+v^2}_{i,j}\right)\right]_{max}, t = 0, t_{end}. \tag{8}$$

are recorded for an analogue of smoke foil tracks. The numerical transverse wave tracks are shown in Fig. 4. Comparing to the results in Lefebvre and Oran (1995) and Oran (1995), much clearer tracks are obtained and the numerical detonation cells show fairly good agreement with the real detonation cells in experiments. The width/length ratio, track angles are close to those measured from the experimental detonation cells of the same gas mixture. Table 1 shows the details of comparisons between the numerical results and the experiments (Strehlow 1968). It is noted that, as the exit angle is rather small and may not be sufficient sharp for an accurate measurement, we chose the

maximum possible value. The absolute size of the cell computed in this case study of $20mm$ channel is about $0.008m \times 0.015m$, which is smaller than that of Oran et al (1998). It is noted too that there are other parameters which have also been used to denote the detonation cells, such as total energy release and maximum pressure (Lefebvre and Oran 1995, Oran et al 1999, Gamzo et al 1999). Our numerical experiments show that the choice of these parameters does not make much difference to the computed transverse wave tracks.

5.3 Evolution of the structure

Since the density changes rapidly across both shock and contact discontinuities, in order to determine the position and details of the triple wave configuration, two dimensional gray scale plots of the density gradient are calculated by

$$|\nabla\rho| = \left[\left(\frac{\partial\rho}{\partial x}\right)^2 + \left(\frac{\partial\rho}{\partial y}\right)^2\right]^{1/2} \tag{9}$$

and is used provide to strengthen the information on the said shocks and contact discontinuities. With these density gradient plots, the evaluation of the structure is shown in Fig. 5 for 4 positions of the shock configuration through the two successive triple collision points A and B. It is observed that, while moving along the transverse track, the shock configurations at all the 4 positions show characteristics of the strong type structure. In Lefebvre and Oran (1995), it was suggested that, after triple collision, the structure begins as a weak type and changes gradually to the strong type at about the half-way mark to the next triple collision. However, our results show that the strong type structure forms just shortly after the triple collision, which is indicated by the shock configuration at position 1-1 in Fig. 5. As our lower resolution results also show similar properties as in Lefebvre and Oran (1995), this apparent discrepancy is likely attribute to the less detailed structure information provided in previous lower resolution studies.

Table 1
Cell geometric parameters vs experimental data

Geometric parameter	current results	experimental data
Width/length (d/l)	0.56	$0.5 \sim 0.6$
Exit angle (β)	$< 10^o$	$5^o \sim 10^o$
Entrance angle (α)	40^o	$32^o \sim 40^o$
Track angle (ω)	29^o	$\sim 30^o$

Through the structure evolution, the angle between the incident wave and the transverse wave track (ϕ) measures in the range of $45^o \sim 50^o$; the angle between the incident wave and the Mach stem (Δ) measures in the range of $40^o \sim 45^o$. Furthermore, it is shown in Fig 5 that the angle between the Mach stem and the track is almost constant and very close to 90^o. By comparing the pressure ratio across the transverse wave, the transverse wave strength (pressure ratio minus one) is found in the range of $1.5 \sim 1.8$ for the strong transverse wave and almost constant at about 0.8 for the weak transverse wave. One can find that these results bear same similarities to Urtiew (1976); that is, the angle ϕ and the transverse wave strength are approximately constant through the cell and the configuration can be considered like an object with a fixed shape moving along the cell track and rotating to keep ϕ constant.

Figure 6 shows the successive instantaneous pressure profiles on the normalized cell centerline. One can observe that, near the cell apex, the shock pressure quickly attains its maximum value and then decays towards the cell end. In the first $0.2l$, the leading front assumes a strong rarefaction process, so the shock pressure declines fairly quickly. Then the rarefaction becomes weaker, the shock pressure declines more slowly. After about $0.85l$, the pressure maximum shifts to a distance behind the leading wave because the collision of the transverse waves induced a new pressure jump. Near the end of the cell, while the triple collision takes place, this pressure maximum jumps to a very high value again, which corresponds to the the collision of the strong and weak transverse waves. One can find that the pressure decay in present results concurs well with Hanana et al's (2000) experimental data. However, the experiments can not properly resolve the pressure profile when the leading wave is around the cell apex.

Even though the Mach stem, the incident wave and the transverse wave of the structure can induce ignition, the three ignition mechanisms are responsible for the different portion of gas mixture in a detonation cell. By comparing the pressure and H_2O concentration plots as the structure evolves, according to the different ignition mechanisms, a detonation cell can be approximately divided into four regions as shown in Fig. 7. In the first region, which is the largest portion of the gas mixture is ignited by the Mach stem; a slightly lesser portion of the gas mixture of the second region is ignited by the incident wave; the transverse waves ignite a yet smaller portion of the gas mixture in the third region; in the triple wave collision region, the smallest portion of gas mixture is ignited by the colliding strong and weak transverse waves in the triple wave collision process. From Fig. 7, one can also observe that as the structure evolves towards the triple collisions, the two transverse waves in a cell ignites more and more portion of the gas mixture due to the lengthening of the induced zone behind the incident wave. In Oran et al (1998), a transverse wave ignition was also suggested, but the predicted ignition begins at about 2/3 of the cell; this is indicated at 1/2 of the cell or just after the triple

collision by the present calculation. A possible reason is that a weak structure whith no transverse wave ignition is suggested in Oran et al (1998), before the formation of strong structure with the igniting transverse wave. In Mitrofanov (1996), the incident wave ignition region (region 2) is ignited by the so called third shock compression, which is caused by the waves after two transverse waves collide. The current results show that only the extending transverse waves collide in region 2. As the extending transverse wave is fairly weak and the incident wave has already ignited the gas mixture, it suggests that there is no ignition after the extending transverse wave collision. This results are consistent with the experimental data of ordinary detonations in Shepherd (2003), which suggest direct ignition behind the incident wave.

5.4 Detonation velocity fluctuation

Even in the midst of small errors or perturbations in the calculations with different time interval, the average detonation velocity is still found to be very close to the CJ value. However, the instantaneous detonation velocity measured with the speed of the leading front shows periodic pulsating characteristic, each period corresponds to the cell characteristic time t_{char} by which the leading wave runs through a detonation cell length l. Figure 8 shows a typical normalized, instantaneous detonation velocity as a function of time and distance. From Fig. 8, one can find that there are two phases of detonation velocity fluctuation: accelerating and decelerating. In the accelerating phase, the detonation leading front accelerates to the maximum value at about $0.05t_{char}$ or $0.05l$. The maximum instantaneous detonation velocity is not stable and oscillates around $1.43D_{CJ}$. In the decelerating phase, similarly to the shock pressure variation, the instantaneous detonation velocity initially decelerates very fast within about $0.35t_{char}$ or $0.4l$. This is followed by a relatively more gradual decelerating process. The turning point of the two different decelerating characteristics is about just after the detonation velocity decelerates to D_{CJ}. Similar to the instantaneous maximum velocity, the minimum detonation velocity also depicts unstable behavior with oscillations occurring around $0.77D_{CJ}$. As the detonation velocity decreases to D_{CJ} in the first half cell and the area of the first half cell is less than that of the second half, it can be concluded that the detonation velocity in a cell is mainly less than D_{CJ} and the detonation state mainly in an underdriven state.

The present detonation velocity fluctuation is consistent with previous observation. In Oran et al (1998), similar high-frequency oscillations at the velocity maximum and minimum have also been observed. Their calculated overall velocity fluctuation is about $1.38 - 0.85D_{CJ}$, which is slightly smaller than the present results. Comparing to the experimental detonation velocity fluctuations, both results show the triple collision is stronger than that of an ordinary

detonation but not as severe as that of a marginal detonation. From Fig. 8, the calculated typical ratio of minimum and maximum detonation velocities is about 1.86. With the relation given in Urtiew (1976), the ratio of maximum to minimum detonation velocities is calculated as about 1.7 from the angles ϕ and Δ of the shock configuration. These values are also larger than 1.4 of an ordinary detonation but smaller than about 2.0 of a marginal detonation. However, as the calculated average detonation velocity is much larger that of a marginal detonation and very close to D_{CJ}, which is the most typical characteristics of an ordinary detonation, our results tend to reflects the evaluation of an ordinary detonation rather than a mixed marginal and ordinary behavior (Oran et al 1998). On the disagreements with experimental data of ordinary detonation, it may due to the low resolution measurement for velocity in experiments. Usually, as the velocity measurement can only reflect the local average value, the velocity fluctuation during the rapid rise and fall region near the triple collision is likely to be underestimated compared to the slower process in other parts of the cell. This is similar to the fact that, when the detonation is calculated with much lower resolution, smaller detonation velocity maximum is obtained. For example, in the current work, the calculated detonation velocity maximum is only about $1.35D_{CJ}$ with the grid size of $0.2mm$. In Oran et al (1998), it was also observed that the maximum energy release of the finer grid calculation is much larger than that of coarse solution and tends to form a stronger Mach stem with the higher speed leading front after the triple collision.

6 Conclusion remarks

In this paper, two dimensional numerical simulation of regular detonation cellular structure in $H_2/O_2/Ar$ mixture with low initial pressure has been performed with a reaction model consisting of elementary chemical reactions. The calculations have been carried out with different grid sizes. Clear and well defined numerical cellular structure and detonation cells have been obtained from the high resolution results. Furthermore, the structure evolving through the cell, which includes shock configuration movement, pressure variation, ignition mechanisms and detonation velocity fluctuation, are discussed.

We have found that, even though the calculated cellular structure is not as strong as that of a marginal detonation, it is still of a strong type structure with stronger transverse wave than the results obtained using simple chemical reaction model. As the strong type structure evolves through the cell, the complex shock configuration moves along the cell track with approximately fixed shape and transverse wave strength. Even as the transverse waves result in a strong ignition, it only occupies a relatively small region and plays a minor role of a cell. This is in agreement with the recent experimental observation

on ordinary detonation reaction zones. As the calculated average detonation velocity is very close to the C-J value, the numerical simulated detonation indicates an ordinary detonation. Finally,on the discussions about the measurement of detonation velocity in experiments and numerical simulations, the present work suggests that the experimental data of instantaneous detonation velocity fluctuation for an ordinary detonation may be underestimated.

References

[1] Fedkiw RP, Merriman B, Osher S (1997) High Accuracy Numerical Methods for Thermal Perfect Gas Flows with Chemistry. *J. Comput. Phys* **132** 175-190

[2] Fickett W, Davis WC (1979) *Detonation* (Berkeley: University of California)

[3] Gamezo VN, Desbordes D, Oran ES. (1999) Formation and Evolution of Two-dimensional Cellular Detonations. *Combust. Flame*, **116** 154-165

[4] Geist A, Beguelin A, Dongarra J, Jiang W, Manchek R, Sunderam, V (1994) PVM 3 user's guide and reference manual. *ORNL/TM-12187*

[5] Gordon S, McBride B J (1971) Computer Program for Calculation of Complex Chemical Equilibrium Compositions, Rocket Performance, Incident and Reflected Shocks, and Chamman-Jouget Detonations. *NASA SP273*

[6] Hanana M, Lefebvre MH, Van Tiggelen, PJ (2000) Preliminary Experimental Investigation of Pressure Evolution in Detonation Cells. *Exp. Therm. Fluid Sci.* **21** 64-70

[7] Jiang GS, Shu CW (1996) Efficient Implementation of Weighted ENO Schemes. *J. Comput. Phys* **126** 202-228

[8] Lefebvre MH, Oran ES (1995) Analysis of shock structures in regular detonation. *Shock Waves* **4** 277-283

[9] Mitrofanov VV (1996) Modern view of gaseous detonation mechanism. *Prog. in Astro. and Aero.* vol 137 (Washington, DC: AIAA) p 327-339

[10] Oran, E S, Boris, J P (1987) *Numerical Simulation of Reactive Flow* (New York:Elsevier)

[11] Oran ES, Weber JE, Stefaniw EI, Lefebvre MH, Anderson JD (1998) A Numerical Study of Two-dimensional H2-O2-Ar Detonation Using A Detailed Chemical Reaction Model. *Combust. Flame* **113** 147-163

[12] Quirk JJ (1993) Godunov-type schemes applied to detonation flows *AD-A265482*

[13] Schott GL (1965) Observation of the structure of spinning detonation *Phys. Fluids* **8** 850-865

[14] Sharpe GJ (2001) Transverse waves in numerical simulations of cellular detonations *J. Fluid Mech.* **447** 31-51

[15] Shepehrd JE, Pintgen F, Austin JM, Eckett CA (2003) The structure of the detonation front in gases. *AIAA-2002-0773*

[16] Shu CW, Osher S (1989) Efficient implementation of essentially non-oscillatory shock-capturing schemes, II. *J. Comput. Phys* **83** 32-78

[17] Strehlow RA, Crooker AJ (1974) The structure of marginal detonations. *Acta Astronautica* **1** 303-315

[18] Strehlow RA (1968) Gas phase detonations: recent developments. *Combust. Flame* **12** 81-101

[19] Stull DR (1971) *JANAF Thermochemical Tables, National Standard Reference Data Series, No. 37. 2nd Ed.* (Gaithersberg: U. S. National, Breau of Standrads)

[20] Taki S, Fujiwara, T (1978) Numerical Analysis of Two-Dimensional Nonsteady Detonations. *AIAA Journal*,**16** 73-77

[21] Voitsekhovskii BV, Mitrofanov VV, Topchian ME (1966) Struktura fronta detonatsii v gazakh (Structure of a detonation front in gases). *AD-633821*

[22] Urtiew PA (1976) Idealized two-dimensional detonation waves in gaseous mixture *Acta Astronautica* **3** 187-200

[23] Wilson GJ, MacCormack RW (1990) Modeling supersonic combustion using a fully-implicit numerical method *AIAA-90-2307*

[24] Young TR (1979) CHEMEQ-Subroutine for solving stiff ordinary differntial equtions *AD-A0835545*

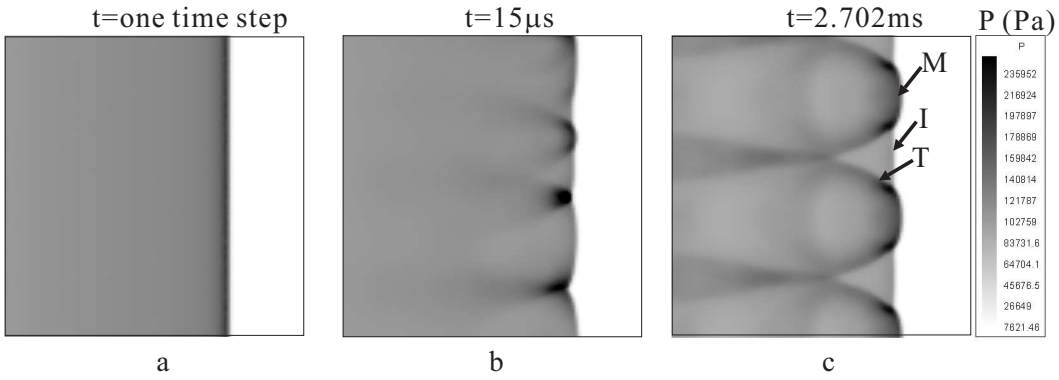

Fig. 1. Pressure contours at 3 different times; M: Mach stem, I:incident wave, T: transverse wave

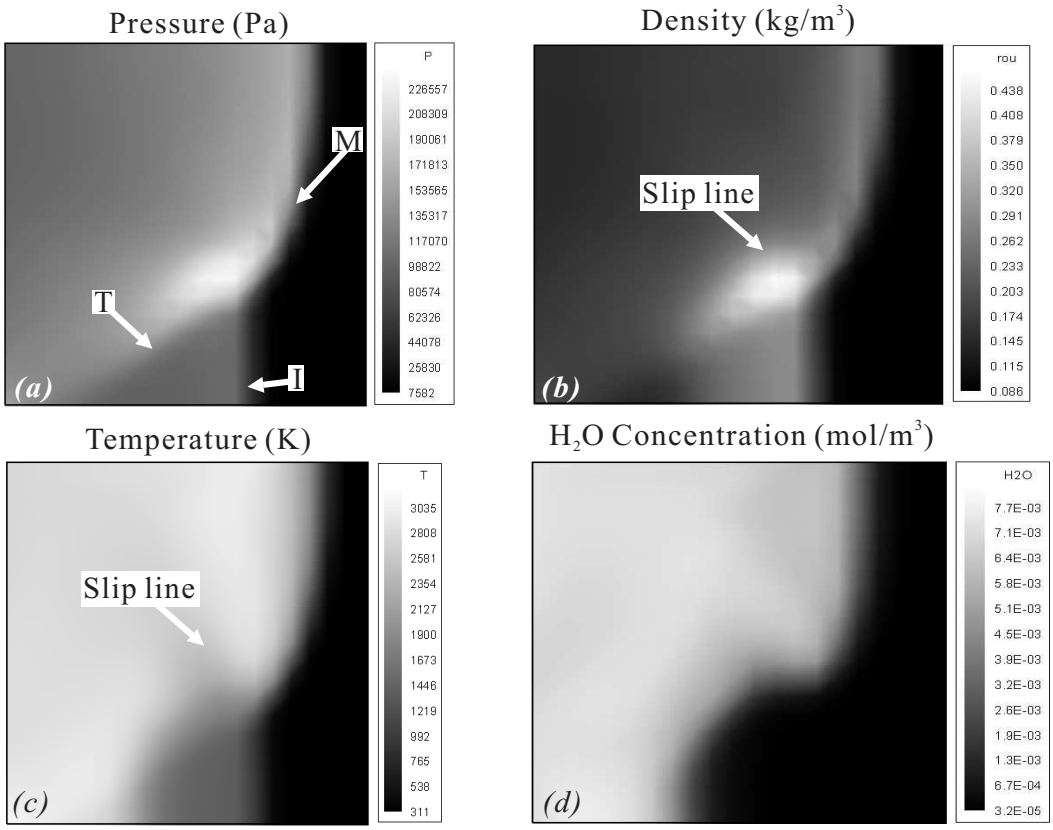

Fig. 2. Regular cellular structure with 0.2mm grid size; a)pressure, b)density, c)temperature, d)H_2O concentration

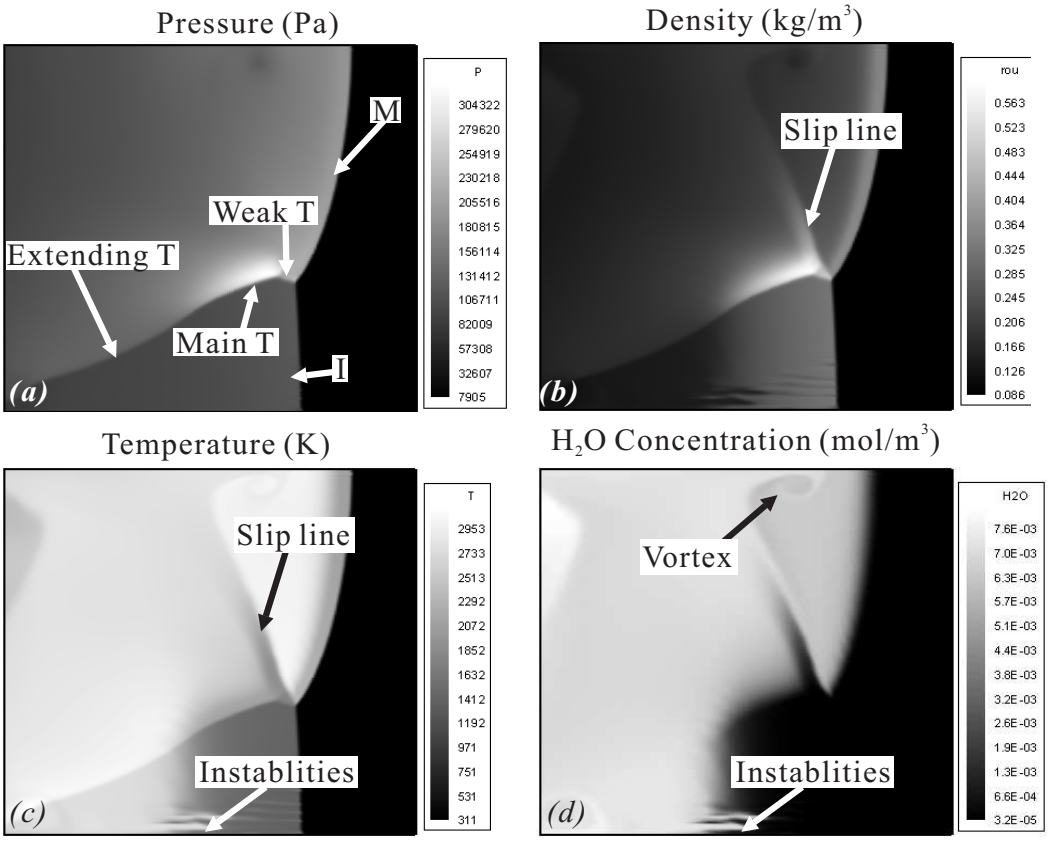

Fig. 3. Regular cellular structure with $0.025mm$ grid size; a)pressure, b)density, c)temperature, d)H_2O concentration

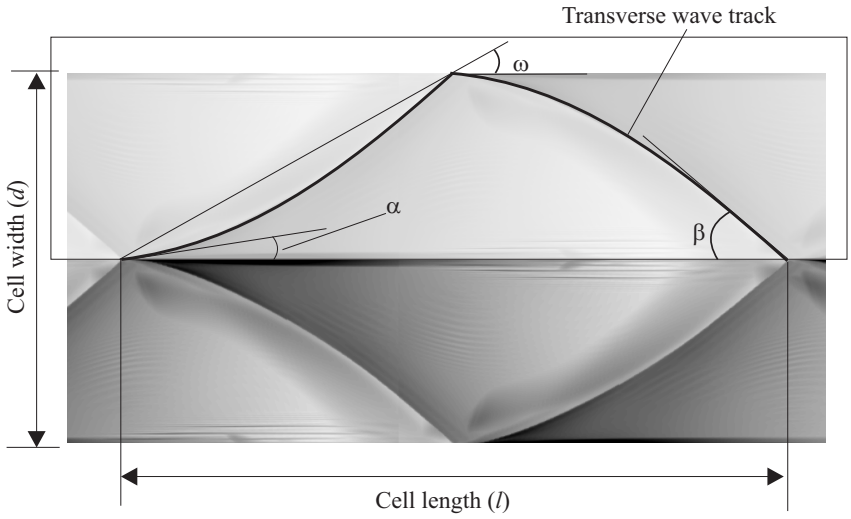

Fig. 4. Geometric parameters of a numerical cell

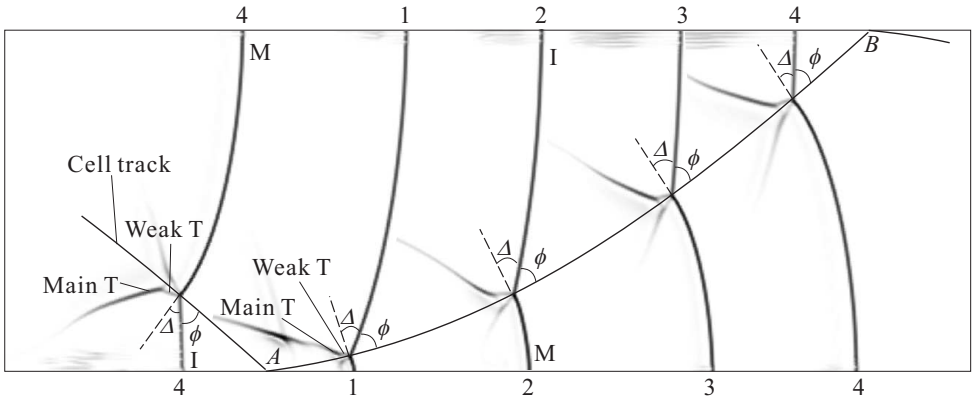

Fig. 5. Structure evolution through the cell

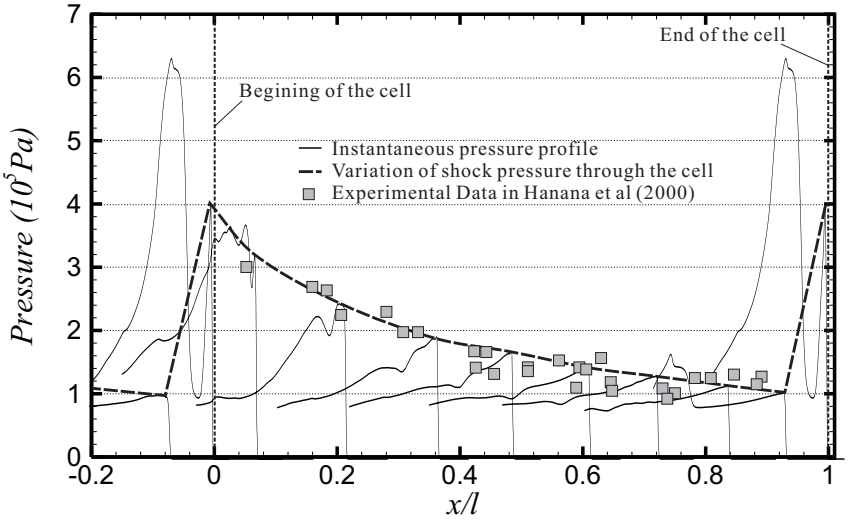

Fig. 6. Variation of pressure on the normalized cell central line

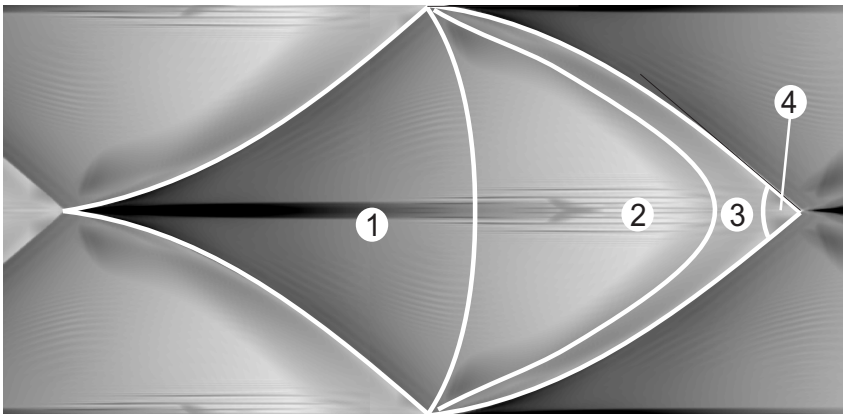

Fig. 7. Divided cell according to the ignition mechanisms (the background is a numerical detonation cell); 1)Mach stem, 2)Incident wave, 3)Transverse wave, 4)colliding of strong and weak transverse waves

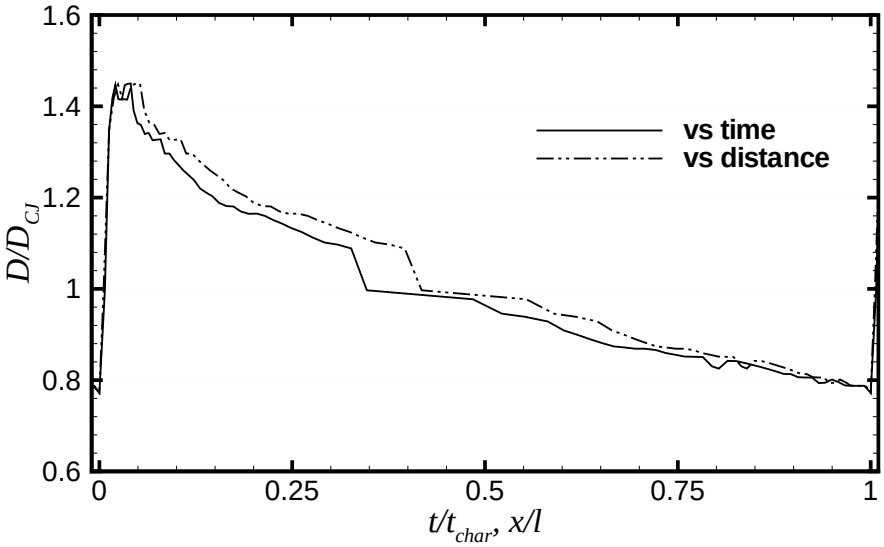

Fig. 8. The normalized instantaneous detonation velocity along the cell central line